AJNR

Magnetic susceptibility artifact in spin-echo MR imaging of the pituitary gland.

K Sakurai, N Fujita, K Harada, S W Kim, K Nakanishi and T Kozuka

Magnetic Susceptibility Artifact in Spin-Echo MR Imaging of the Pituitary Gland

Kosuke Sakurai,[1] Norihiko Fujita,[1] Koushi Harada,[1] SangWon Kim,[2] Katsuyuki Nakanishi,[1] and Takahiro Kozuka[1]

PURPOSE: To evaluate the magnetic susceptibility effect on spin-echo MR images of the pituitary gland. METHODS: Air-in-water phantom experiments and studies in normal volunteers were performed using various sampling bandwidth (8.3–33.3 kHz) spin-echo sequences with the polarity of the readout gradient normal or reversed. RESULTS: Attachment of a sphenoid septum to the sellar floor was the major factor in the appearance of the inferior surface of the pituitary gland. Patterns of distortion and/or artifactual signal intensities, related to the presence or absence of the attachment, were accentuated on the images with narrower bandwidth. A "spearhead shape" deformity of the sphenoid sinus was observed both in the air-in-water phantom experiment, and when no sphenoid septum was present. When a sphenoid septum was present, two spearhead shapes side by side were present. High-intensity artifacts were seen where the sellar floor was misplaced into the pituitary gland. CONCLUSION: Knowledge of the patterns of distortion and high-intensity artifact is important in the diagnosis of pituitary lesions.

Index terms: Pituitary gland, magnetic resonance; Magnetic resonance, artifacts; Magnetic resonance, physics

Magnetic resonance imaging (MR) is the modality of choice for sellar-parasellar imaging because of its excellent ability to demonstrate anatomical structures (1–3). However, since abundant air-tissue interfaces are present near the pituitary gland, considerable local perturbations of the resonant frequency are caused by the presence of large magnetic susceptibility differences. Even with the use of spin echo rather than gradient field echo pulse sequences, the local frequency perturbations will lead to geometric distortions and artifactual signal intensity changes (4, 5). These magnetic susceptibility effects are more prominent on high-field systems in the same way as are chemical shift artifacts (5), since these effects are characterized by the term "off-resonance effects," ie, perturbations of the reso-

nant frequency that are proportional to the applied magnetic field. Using a 1.5-T unit, we frequently observed a high-intensity spot (Fig. 1) on T1-weighted images at the junction of the sellar floor and a septum of the sphenoid sinus. Kaufman et al (6) reported that this high-intensity spot is an artifact that is a result of image distortion due to large magnetic susceptibility differences. This artifact has been reported to depend on the sampling bandwidth, direction of the static magnetic field, and the presence of the sphenoid septum (6).

As is seen in the chemical shift artifacts, image distortion due to frequency perturbations depend on the sampling bandwidth and the readout gradient direction (4). For example, reduction of sampling bandwidth leads to the increase of misplacement caused by the frequency perturbations and reversal of the polarity of readout gradient results in the misplacement to the opposite side.

The purpose of this article is to evaluate the effects of magnetic susceptibility in spin-echo imaging of the sellar region and to illustrate the patterns of distortion that depend on the presence or absence of the sphenoid septum, various sam-

pling bandwidth, and the polarity of the readout gradient.

Materials and Methods

To evaluate the magnetic susceptibility effects in the sellar region, images of air-in-water phantom and the pituitary glands of four normal volunteers were obtained with variable bandwidth spin-echo sequences shown in Table 1. All images were obtained with a Magnetom 1.5 T (Siemens, Erlangen, Germany). The direction of the static magnetic field is horizontal (craniocaudal) direction, which is parallel or antiparallel to the readout gradient on coronal images.

Pulse Sequences

In commercially available sequences, standard bandwidth used for T1-weighted and proton density-weighted images is 33.3 kHz (sequence C), and reduced bandwidth 16.7 kHz (sequence B) is used to improve signal-to-noise
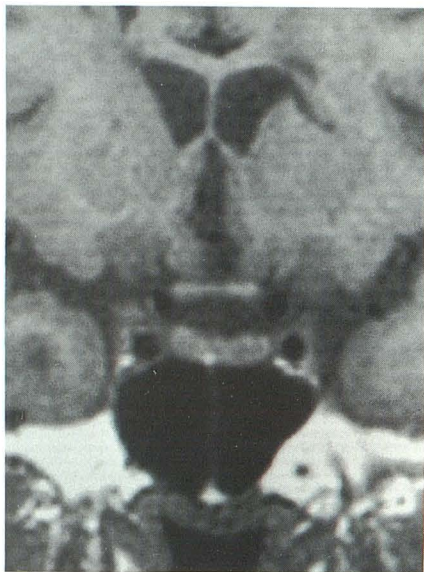

Fig. 1. High-intensity spot artifact: High-intensity spot is seen at the junction of the sellar floor and septum of the sphenoid sinus. This artifact is thought to be the result of magnetic susceptibility effect. A linear low-intensity hemorrhagic infarct is seen in the left caudate nucleus and internal capsule. This was of low signal intensity on T2-weighted image.

TABLE 1: Table of pulse sequence

	Readout Direction	Sampling Bandwidth (kHz)
Sequence A	N	8.3
Sequence A'	R	8.3
Sequence B	N	16.7
Sequence B'	R	16.7
Sequence C	N	33.3
Sequence C'	R	33.3

Note.—N, normal readout gradient; R, reversed readout gradient.

ratio for T2-weighted images. Sequence A with bandwidth 8.3 kHz was specially made to accentuate the misregistration due to magnetic susceptibility effects.

For each sequence shown in Table 1, the prime sign (') denotes the reverse of polarity of the readout gradient. In the "normal" readout gradient, frequency-encoded direction is vertically upward, with higher side of gradient to the bottom on coronal images, while in the "reversed" readout gradient, it is vertically downward, with higher side of gradient to the top.

Phantom Experiment

To visualize the effect of air to surrounding water, which simulates the presence of air in the sphenoid sinus, we made a simple air-in-water phantom and a chemical shift phantom (Fig. 2). The air-in-water phantom consisted of a cylindrical water container (14.5 cm) in which a smaller (5 cm) container of spherical shape was placed. The smaller phantom was made of glass with a 1-mm wall and filled with air. The magnetic susceptibility of glass is approximately equal to that of water (7). The chemical shift phantom consisted of two cylinders (4 cm and 1 cm). The inner cylinder was filled with olive oil and the outer cylinder with water. These cylinders were also made of glass with a 1-mm wall. These phantoms were imaged at bandwidths 8.3, 16.7, and 33.3 kHz with normal readout gradient (sequences A, B, and C in Table 1) and reversed readout gradient at each bandwidth (sequences A', B', and C' in Table 1). The imaged slice was horizontal at the center of the spherical air, which corresponds to the coronal plane in the human body.

In sequence A and A' (8.3 kHz), sampling time was prolonged to 30.72 msec corresponding to a 256 matrix in frequency-encoded axis, and the minimal necessary TE was 40 msec. Scan parameters were common in each image except for sampling bandwidth: 500/40/8 (TR/TE/excitations), 256 × 256 matrices, 20-cm field of view, and 5-mm slice thickness.

Volunteer Study

Coronal T1-weighted images of four volunteers (age 20–38 years, mean 25 years) who had no evidence of sellar lesion were obtained at bandwidths 8.3, 16.7, and 33.3 kHz with normal and reversed readout gradient (Table 1). Scan parameters were common in each image except for sampling bandwidth: 500/40/2, 256 × 256 matrices, 20-cm field of view, and 5-mm slice thickness.

On the acquired images, we focused on the shape of the sphenoid sinus, especially on the distortion of the inferior surface of the pituitary gland and the high-intensity spot artifact. We evaluated their relationship to the presence or absence of the sphenoid septum and to the sampling bandwidth.

Results

Phantom Experiment.

Spherical air in water resulted in a "spearhead-shaped" image (Fig. 3). Image distortion and ar-

tifactual signal intensities were observed, which were more prominent at narrow bandwidth. Chemical shift misregistration was observed, which was inversely proportional to the sampling bandwidth. The direction of chemical shift mis-
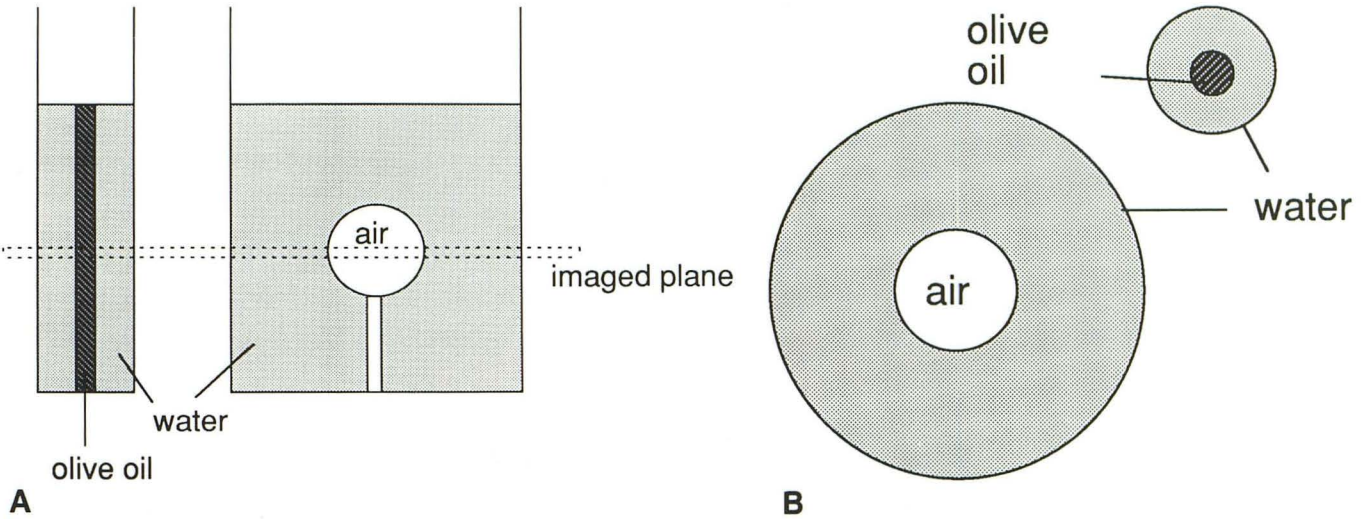

A

B

Fig. 2. *A*, Schematic illustration of air-in-water phantom and chemical shift phantom. *B*, Arrangement of phantoms in the imaged plane. Spherical air phantom was placed in cylindrical water phantom. The imaged plane was horizontal at the center of the sphere. These phantoms were made of glass with 1-mm walls thick.
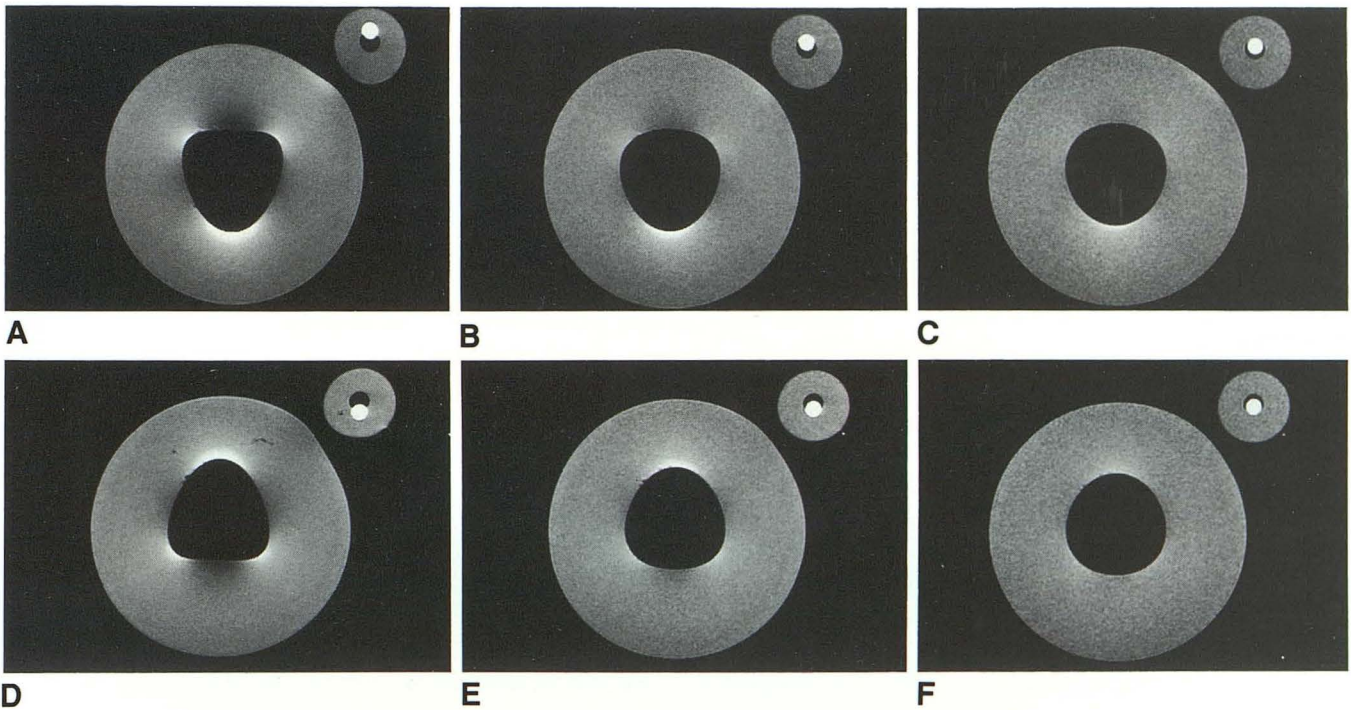

A   **B**   **C**

D   **E**   **F**

Fig. 3. Distorted image of air-in-water phantom: *A* and *D* were imaged at the bandwidth 8.3 kHz; *B* and *E* at 16.7 kHz; *C* and *F* at 33.3 kHz. Direction of the readout gradient was normal (vertically upward) in *A*, *B*, and *C*, and was reversed (vertically downward) in *D*, *E*, and *f.* Sphere air in water was imaged as a "spear-head shape." This spearhead always pointed to higher side of gradient. Image distortion was more prominent at narrower bandwidth. Chemical shift misregistration indicates the direction of readout gradient and the amount of misregistration indicates the sampling bandwidth. The outer borders of the two water cylinders are slightly distorted at narrower bandwidth, because the two water cylinders in air distort the magnetic field in the air and affect each other.

registration indicates the direction of readout gradient. Using the reversed readout gradient, the spearhead points to the opposite, higher side of the gradient.

Volunteer Study

Attachment of sphenoid septum to the sellar floor was present in three of four volunteers.

In these three cases, high-intensity spot artifacts at the junction were seen with sequences A, B, and C (Figs. 4A, 4B, and 4C). With use of reversed readout gradient (sequences A', B', and C'); however, these high-intensity spot artifacts disappeared and linear high-intensity artifacts appeared along the inferior surface of the pituitary gland, except at the point of junction with the sphenoid septum (Figs. 4D, 4E, and 4F). High-intensity spot artifacts and distortion of the inferior surface of the pituitary gland were more prominent in narrower bandwidth sequences. The point where the sphenoid septum makes junction with the sellar floor shifted into the pituitary gland in sequence A, and into sphenoid sinus in sequence A'. The adjacent sellar floor appeared as a convex shape in sequence A, and a concave shape in sequence A'. These patterns of distortion and high intensities were seen in all volunteers.

In the other case that had no attachment of sphenoid septum (Fig. 5), the inferior surface of the pituitary gland appeared convex and had relatively low signal intensity in sequence A. Using reversed readout gradient, it appeared concave with linear high intensity.

Discussion

In substances other than ferromagnets, the presence of an external magnetic field induces the magnetization proportional to the magnitude of the applied field (8). Magnetic susceptibility χ is the ratio of the intensity of the magnetization to the applied magnetic field. χ is negative for diamagnetic substances and positive for paramagnetic substances. For example, $\chi = -0.72 \cdot 10^{-6}$ for water, and $\chi = 24.1 \cdot 10^{-6}$ for air at 20°C in CGS units (8). Spatial variations in magnetic susceptibility causes frequency perturbations. These frequency perturbations interfere with the imaging gradient fields and, hence, translate into local spatial distortions and artifactual signal intensities on MR images (5). the magnetic susceptibility effect is analogous to the chemical shift

effect in that both effects are characterized by perturbations of the resonance frequency. However, the presence of fat does not affect the frequency of the protons around the adipose tissue. Therefore, only the signal from fat is misregistered on the image, which results in artifactual signal intensity when the misregistered signal overlaps the signal of surrounding water (5, 9). On the contrary, since a small magnet makes inhomogeneous magnetic field around the magnet, the presence of air in water disturbs the magnetic field and affects the processional frequency of the proton around the air. The degree of frequency perturbation spatially varies (4). Thus the presence of air in water leads to the distortion of the water image and an artifactual signal intensity that is caused by image contraction or expansion of surrounding water.

Frequency perturbations due to either magnetic susceptibility or chemical shift effects interfere with the readout gradient and result in misregistration along the frequency-encoded axis. It is well known that reducing the sampling bandwidth increases the degree of misplacement of chemical shift (9). This means that the effects of frequency perturbations depends on the sampling bandwidth. Thus, the geometric distortions and signal intensity changes caused by magnetic susceptibility effects will change when the sampling bandwidth is changed. The relationship between the pixel misplacement n and sampling bandwidth f_{sa} is described as,

$$n = \frac{\Delta f}{\Delta \nu} = \Delta f \cdot \frac{N}{f_{sa}} \qquad (A)$$

where Δf is a frequency perturbation, $\Delta \nu$ is the frequency range over one pixel, and N is the number of pixels in the readout dimension. The relationship between $\Delta \nu$, f_{sa}, and N are determined by the Nyquist condition (10, 11). On the condition that Δf and N are constant, Equation A indicates that the amount of misplacement in pixel number is inversely proportional to the receiver sampling bandwidth. The direction of misplacement depends on the sign of Δf and the direction of readout gradient. Positive Δf corresponds to the misplacement to the higher side of gradient and negative Δf to the lower side of gradient. If reversed readout gradient is used, the direction of misplacement turns to the opposite side on image.

Ludecke previously published the magnetic susceptibility effect using an air-in-water model (4), in which cylindrical or spherical air affects
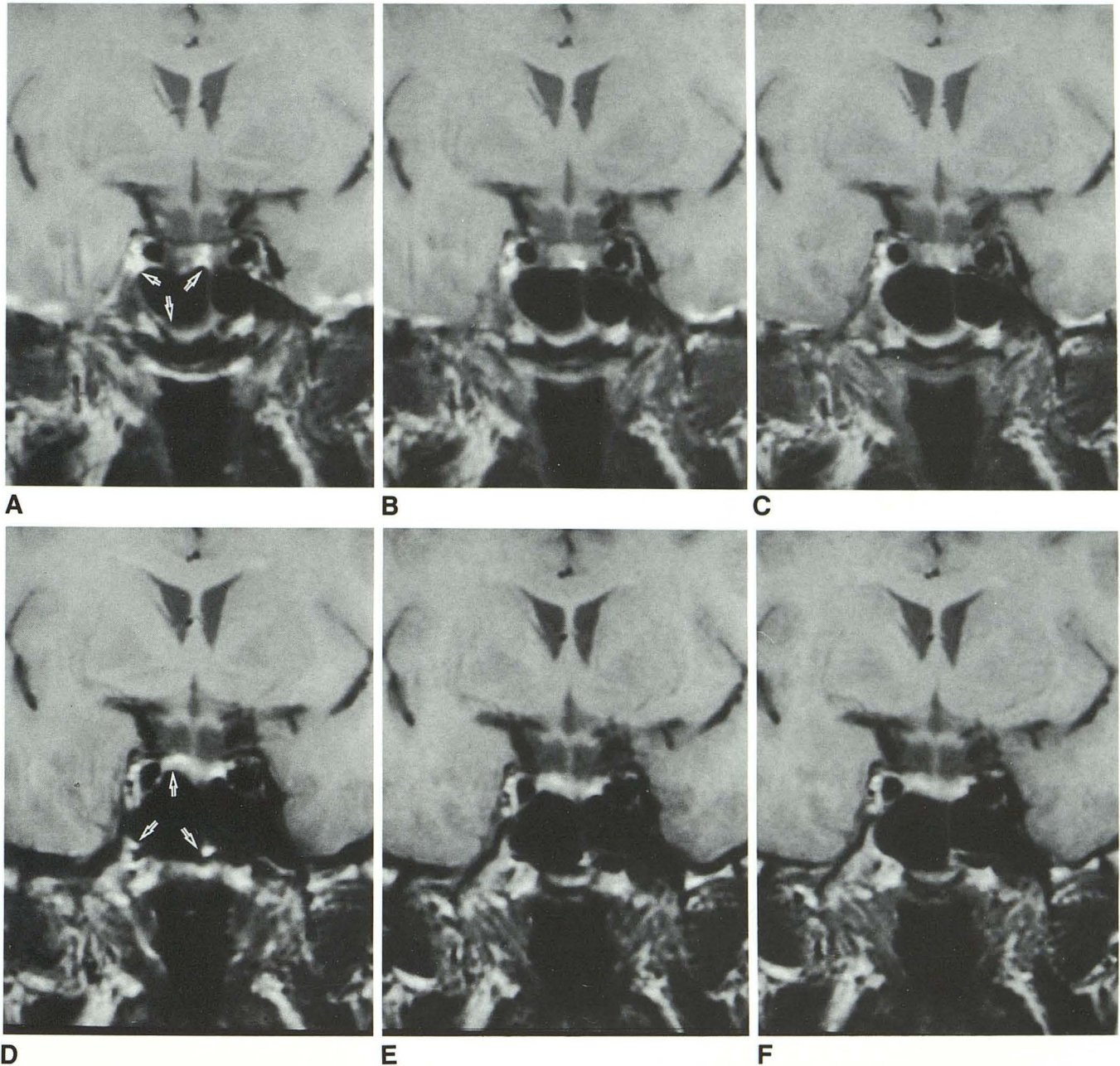
Fig. 4. Distortion of inferior surface surface of the pituitary gland in the cases of attachment of sphenoid septum: *A* and *D* were imaged at the bandwidth 8.3 kHz; *B* and *E* at 16.7 kHz; *C* and *F* at 33.3 kHz. Direction of the readout gradient was normal in *A*, *B*, and *C*, and was reversed in *D*, *E*, and *F*. In normal readout gradient (*A*, *B*, and *C*), the point of attachment shifted into the pituitary gland and high-intensity spot was seen. The other parts of the surface showed downward convex shape. In reversed readout gradient (*D*, *E*, and *F*), the point of attachment shifted into the sphenoid sinus. The other parts showed downward concave. High-intensity spots were seen bilaterally to the point of attachment. The right sphenoid sinus shows spearhead shape in narrow bandwidth sequence (*arrow* in *A* and *D*). The deformity is slightly larger in right side, probably due to larger sinus in right side.

surrounding water to produce a spearhead shape. Our phantom experiment, a spherical air-in-water model, also showed spearhead deformity, to which degree depends on sampling bandwidth. High-intensity areas appear at points A and C in Figure 6. Points B and D show relatively low intensity. Points A and D were misplaced to the

higher side of gradient and point C was misplaced to the lower side of gradient. These high intensities are observed where the border of air and water was misplaced into the water. Thus, high intensities are caused by image contraction (increase of apparent proton density) of surrounding water, and low intensities by image expansion
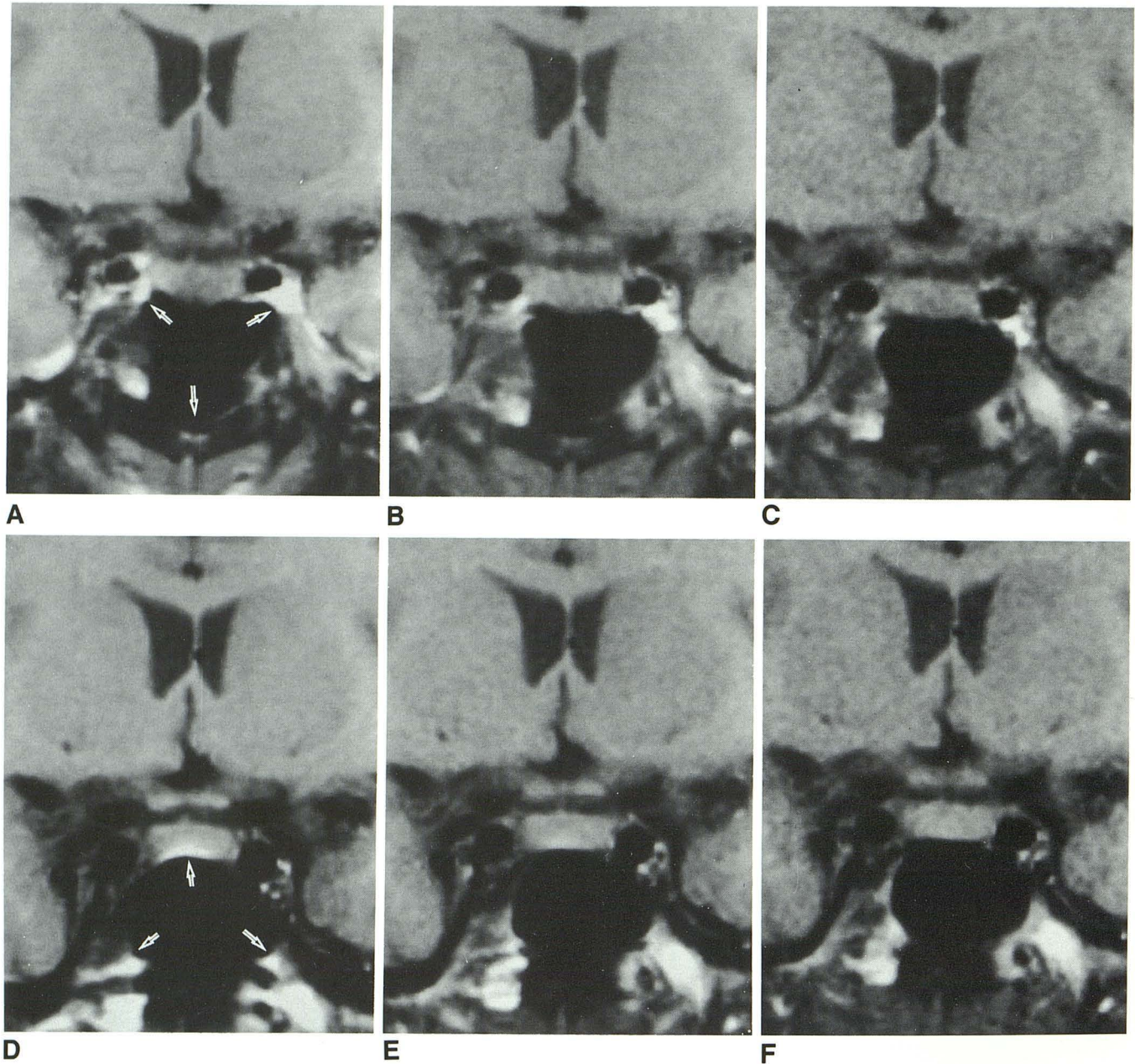
Fig. 5. Distortion of inferior surface of the pituitary gland in the case of no attachment of sphenoid septum: *A* and *D* were imaged at the bandwidth 8.3 kHz; *B* and *E* at 16.7 kHz; *C* and *F* at 33.3 kHz. Direction of the readout gradient was normal (vertically upward) in *A*, *B*, and *C*, and was reversed (vertically downward) in *D*, *E*, and *F*. In normal readout gradient (*A*, *B*, and *C*), the inferior surface showed downward convex shape. High-intensity spot was not seen. In reversed readout gradient (*D*, *E*, and *F*), the inferior surface showed downward concave shape. Linear high intensity was seen along the inferior surface. The sphenoid sinus shows spearhead deformity (*arrow* in *A* and *D*) similar to Figure 3.

(decrease of apparent proton density), where the border was misplaced into the air (4).

Figure 7 schematically represents the results of normal volunteer studies. Patterns of distortion of the inferior surface of the pituitary gland was dependent on the direction of readout gradient and presence or absence of the sphenoid septum. These patterns consist of spearhead-shape de-

formities of the sphenoid sinus. High-intensity areas appeared where the inferior surface was misplaced into the pituitary gland.

In the case of no attachment, the sphenoid sinus appeared as a single spearhead shape, which is similar to the images of phantom in Figure 3. The inferior surface of the pituitary gland appeared downward convex in normal
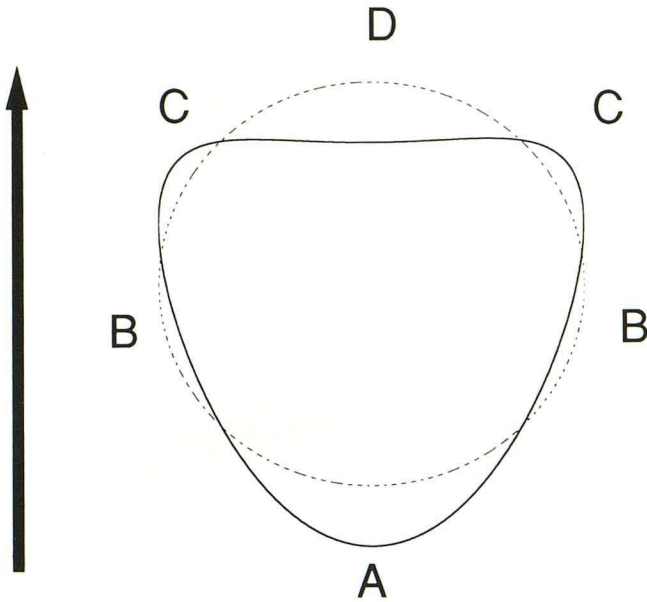
Fig. 6. Sketch of the distorted image of air-in-water phantom (Fig. 3A). *Dashed circle* represents the "true" border between air and water and *solid line* represents the imaged border. *Arrow* indicates the direction of the readout gradient. Points *A* and *C* showed high intensity and *B* and *D* showed low intensity.
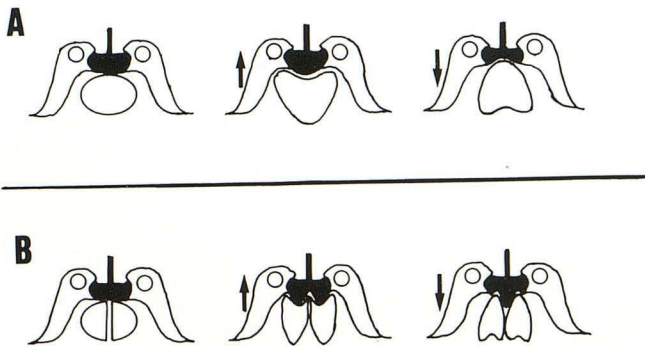

Fig. 7. Schematic illustration of the result of normal volunteer study. Series *A* is the result of one case in which sphenoid septum was absent and series *B* represents the three cases in which sphenoid septum was present. In each series, left schema means the object to be imaged, center is imaged with normal readout gradient, and right is imaged with reversed readout gradient. *Arrows* denote the direction of readout gradient.

readout gradient, which corresponds to point D in Figure 6, and convex in reversed readout gradient, which corresponds to point A. The linear high intensity observed along the inferior surface in reversed readout gradient is explained by the signal overlapping due to image contraction.

In the cases of attachment, phenomena are more complicated corresponding to the complex structure of the sella and sphenoid sinus. The point that is a junction of sellar floor and sphenoid septum is misplaced to the lower side of gradient. The adjacent portion of the floor was convex

downwards with the normal readout gradient and concave with the reversed readout gradient. These complicated deformities are understood with the analogy to spearhead-shape deformity; that is, two spearheads are arranged side by side. The junctional point corresponds to each point B of two spearheads, which is misplaced to the lower side of gradient. The other part of sellar floor corresponds to point A in normal gradient, to point C in reversed.

In clinical imaging, as was pointed out by Kaufman et al (6), this high-intensity spot artifact can be misinterpreted as a normal structure or as a lesion which shows high signal intensity on T1-weighted image: eg, posterior lobe, epithelial rests, hemorrhagic lesions, and some kinds of cystic lesions (3). These normal or pathologic structures would not, however, change their appearance when sampling bandwidth or direction of readout gradient was changed. This high-intensity spot is one of those artifacts that one quickly learns to "see through."

Both this high-intensity spot artifact and the distortion of the inferior surface of the pituitary gland can be misinterpreted. Although down-sloped sellar floor is one of the signs that suggests the presence of microadenoma (2, 12, 13), patterns of artifactual distortion of the inferior surface of the pituitary gland must be taken into consideration. Furthermore, measurements of the height of the pituitary gland, which are obtained during MR (14, 15) as well as CT to determine the size of the gland, can also be affected by this distortion. The measured values can be changed by many factors: magnitude of static magnetic field, static field inhomogeneity, structure of sphenoid sinus, sampling bandwidth, and direction of readout gradient and static field. Thus, these values of measurement in frequency-encoded direction are, to a moderate degree, technically dependent.

Increasing bandwidth is the only way to reduce or eliminate these misplacement artifacts; however, images with increased sampling bandwidth suffer from low signal to noise ratio (16, 17), which can be a problem when it is necessary to obtain this-section high-resolution images. It is difficult to completely eliminate these off-resonance artifacts in acceptable scanning time. In our institute, 50-kHz normal directional readout pulse sequence is routinely used for pituitary imaging. Using this sequence, although off-resonance artifacts cannot be eliminated, chemical shift misplacement is about 1 pixel. Frequency

misregistration due to air-water magnetic susceptibility difference is similar to that of chemical shift (4). Thus misplacement due to magnetic susceptibility difference is considered 1 or 2 pixels, which is taken into consideration in the diagnosis. In our experience, this sequence provides us images with smaller distortion and adequate signal-to-noise ratio in reasonable scanning time. For systems of magnetic field other than 1.5 T, sampling bandwidth can be determined with reference to frequency perturbation due to chemical shift, which is proportional to the strength of static magnetic field.

In conclusion, the appearance of sellar floor is greatly affected by sampling bandwidth, direction of readout gradient, and presence of sphenoid septum. The knowledge of the patterns of distortion and high-intensity artifact is important in the diagnosis of pituitary lesions.

References

1. Lee BCP, Deck MDF. Sellar and juxtasellar lesion detection with MR. *Radiology* 1985;157:143–147
2. Bilaniuk LT, Zimmerman RA, Wehrli EW, et al. Magnetic resonance imaging of pituitary lesions using 1.0 to 1.5 T field strength. *Radiology* 1984;153:415–418
3. Kucharczyk W. The pituitary gland and sella turcica. In: Brant-Zawadzki M, Norman D, eds. *Magnetic resonance imaging of the central nervous system*. New York: Raven, 1987:187–208
4. Ludecke KM. Susceptibility Artifacts in NMR imaging. *Magn Reson Imaging* 1985;3:329–343
5. Bellon EM, Haacke EM, Coleman PE, Sacco DC, Steiger DA, Gangarosa RE. MR artifacts: a review. *AJR* 1986;147:1271–1281
6. Kaufman B, Kormos DW, Clampitt ME, Haacke EM. Paper presented at the 7th annual meeting of the Society of Magnetic Resonance in Medicine, San Francisco, CA, August 1988
7. *Chronological scientific tables.* Edited by Tokyo Astronomical Observatory. Tokyo: Maruzen, Japan, 1984:531
8. Lorrain P, Corson DP, Lorrain F. *Electromagnetic fields and waves.* 3rd ed. New York: Freeman, 1988:360–372
9. Smith AS, Weinstein MA, Hurst GC, DeRemer DR, Cole RA, Duchesneau PM. Intercranial chemical-shift artifacts on MR images of the brain: observations and relation to sampling bandwidth. *AJNR* 1990;11:303–311
10. Bracewell RN. The Fourie transform and its applications. 2nd ed. New York: McGraw-Hill, 1986:189–194
11. Haacke EM. Image behavior: resolution, signal-to-noise, contrast, and artifacts. In: Modic MT, Masaryk TJ, Ross JS, eds. *Magnetic resonance imaging of the spine*. Chicago: Year Book, 1989:5, 14–16
12. Kulkarni MV, Lee KF, McArdle CB, et al. 1.5 T MR imaging of pituitary microadenomas: technical considerations and CT correlation. *AJNR* 1988;9:5–11
13. Peck WW, Dillon WP, Norma D, Wilson CB. High-resolution MR imaging of pituitary microadenomas at 1.5 T: experience with Cushing disease. *AJNR* 1988;9:1085–1091
14. Suzuki M, Takashima T, Kadoya M, et al. Height of normal pituitary gland on MR imaging: age and sex differentiation. *J Comput Assist Tomogr* 1990;14:36–39
15. Elster AD, Chen MYM, Wiliams DW III, Key LL. Pituitary gland: MR imaging of physiologic hypertrophy in adolescence. *Radiology* 1990;174:681–685
16. Vinitski S, Griffey R, Fuka M, Matwiyoff N, Prost R. Effect of sampling rate on magnetic resonance imaging. *Magn Reson Med* 1987;5:278–285
17. Hendrick RE. Sampling time effects on signal-to-noise and contrast-to-noise ratios in spin-echo MRI. *Magn Reson Imaging* 1987;5:31–37